Drying Technology

An International Journal

ISSN: 0737-3937 (Print) 1532-2300 (Online) Journal homepage: https://www.tandfonline.com/loi/ldrt20

Characterization and drying kinetics of iron ore pellet feed and sinter feed

T. C. Souza Pinto, A. S. Souza, J. N. M. Batista, A. M. Sarkis, L. S. Leal Filho, T. F. Pádua & R. Béttega

To cite this article: T. C. Souza Pinto, A. S. Souza, J. N. M. Batista, A. M. Sarkis, L. S. Leal Filho, T. F. Pádua & R. Béttega (2020): Characterization and drying kinetics of iron ore pellet feed and sinter feed, Drying Technology, DOI: 10.1080/07373937.2020.1747073

To link to this article: https://doi.org/10.1080/07373937.2020.1747073

DRYING TECHNOLOGY
https://doi.org/10.1080/07373937.2020.1747073

Characterization and drying kinetics of iron ore pellet feed and sinter feed

T. C. Souza Pinto[a], A. S. Souza[b], J. N. M. Batista[b], A. M. Sarkis[a], L. S. Leal Filho[c], T. F. Pádua[b], and R. Béttega[b]

[a]Instituto Tecnológico Vale - ITV, Ouro Preto, MG, Brazil; [b]Department of Chemical Engineering, Federal University of São Carlos, São Carlos, SP, Brazil; [c]Mining and Petroleum Department, Polytechnic Engineering School, University of São Paulo, São Paulo, SP, Brazil

ABSTRACT

The moisture content of iron ore must be suitable for safe handling and transporting operations. Here, the characterization and drying kinetics of iron ore concentrates were presented and recommendations for the design of dryers were discussed. Pellet feed and sinter feed showed a high amount of fine particles (8–20% d_p<10 μm) and a low pore volume (V_{pore}<10 μm). An ample period for drying at constant rate was observed (critical moisture around 5%), indicating that drying processes aiming at a moderate moisture reduction could be performed within this period. These findings contribute to the design of dryers and support economic operations.

ARTICLE HISTORY
Received 24 October 2019
Revised 18 March 2020
Accepted 22 March 2020

KEYWORDS
Iron ore concentrates; drying kinetics; transportable moisture limit; mineral processing

Introduction

Iron ore is the primary source of metallic iron for industries and is mostly used in the production of steel. The mining of iron ore generally involves the exploitation, grinding, and beneficiation of the material, and then dumping of waste. The final concentrate is usually presented in three main products, depending on the size distribution: coarse (lump ore), medium (sinter feed), and fine (pellet feed). According to the United States Geological Survey (USGS, 2019),[1] the global prices of iron ore products have recently trended down, which is especially concerning because the mining and transport sectors require high investments in equipment and infrastructure such as heavy machinery, off-road trucks, railroads, and bulk carrier ships. In these circumstances, the competitiveness of mining companies is strongly linked to the production costs and the quality of the commodity. For these reasons, it is fundamental to study and develop mining technologies aiming at cost reduction along the iron ore production chain, ensuring sustainability and viability in long-term operation.

The moisture content has several consequences in the iron ore production chain. The amount of moisture present in the material can vary according to the natural state of the ore at the exploitation stage, climatic conditions or other environmental aspects, and according to the processing route, e.g., wet processing, natural moisture or dry processing. A high moisture level can be particularly useful to minimize the generation of dust (specially for fine particles) and consequent loss of product during railroad transportation from the mining sites to ports. However, at the port terminals, the moisture level of the material must meet the regulatory limit for transporting bulk solids in ships in order to ensure safe handling operations. This parameter is known as the Transportable Moisture Limit (TML).[2,3] When the moisture grade of the iron ore is above the identified limit of TML, loading operation must be interrupted, which causes delays and large financial losses. Furthermore, a high level of moisture in the iron ore increases the shipping cost, due to the null cargo weight of water,[4] while decreasing the trading value.

Another issue concerning the moisture content of the iron ore can be found in the pelletizing operation. In the pelletizing plants, the fine portion of iron ore (pellet feed) is mixed with binder agents and then rolled in disks or drums to produce balls of iron oxide (green pellets). These balls are dried and fired before sending them to direct reduction. The quality of the pellets is highly dependent on the moisture content and the size distribution of the fine ores in the feed, as well as on the chemical composition and amount

CONTACT R. Béttega bettega@ufscar.br Department of Chemical Engineering, Federal University of São Carlos, São Carlos, SP, Brazil.
Supplemental data for this article is available online at https://doi.org/10.1080/07373937.2020.1747073.

Table 1. Properties of the materials.

Material	Pellet feed	Sinter feed
Real density (g/cm^3)	4.88	4.92
Apparent density (g/cm^3)	4.09	4.30
Composition		
Fe (%)	64.00	66.30
SiO_2 (%)	2.77	0.80
Al_2O_3 (%)	1.66	0.85
P (%)	0.05	0.06
Mn (%)	0.28	0.08
LOI (%)	2.98	2.90

of binder agents.[5] In order to assist the formation of quality green pellets, it can be necessary to dewater the pellet feed to a moisture content of about 8.5 to 10% before pelletizing, with the value varying according to the type and particle size distribution of the ore.[5] High moisture levels in the pellet feed are detrimental to the green pellet production chain, causing considerable losses of production and energy efficiency, especially for subsequent reduction operations in blast furnaces.

Although some studies have reported the drying of green pellets,[6–14] little is known on the drying of iron ore pellet feed or sinter feed concentrates. Studies concerning the dewatering of these materials are of major interest because the mining industry has been facing new scenarios. In a context of lower grade ores and deeper mines, there is a concern of reducing the tailings either by reprocessing or dewatering, aiming at long term sustainability and economic viability. In the wet iron ore processing, the concentrate leaves the process as a pulp with high moisture content.[15] Reports regarding conventional iron ore dewatering techniques[16] showed improvements in dewatering using new filtering technologies, filtration aids,[17] and surfactants in paste thickeners.[18] However, the final moisture grades achieved by filters and paste thickeners are still high considering handling or transporting the tailings and the final products. Namkung and Cho[19] reported the drying and hydrodynamic characteristics of iron ore with particle diameters ranging from 0.5 to 2.0 mm, which was dried in a vertical pneumatic conveying drier. Ghoshdastidar *et al*[20] developed a model based on heat transfer for the design of a rotary kiln heater and dryer[21] for iron ore with an initial moisture content of 19%. Gas temperature was of 1065 °C at the inlet and about 120 °C at the outlet for a dry solids flow rate of around 4 t/h. The model predicted the length of the kiln and the axial solid and gas temperatures with reasonably good accuracy. Hence, there are very few studies that have investigated the drying or dewatering of iron ore concentrates.

The development of more efficient dewatering and drying systems is in accordance with the requirements of the mining sector, for industrial and commercial purposes. The thermal removal of water during mineral processing is an inevitable future trend in this area, so there is a need to focus on energy efficiency and selection of the most cost-effective systems.[4,16] The desired moisture grade of iron ore concentrates is a sensitive parameter, since low moisture values can lead to dust generation and, on the other hand, the excess of moisture can affect pile stability and cargo loading. For these reasons, a moderate moisture reduction achieved by drying operations is of paramount interest. Despite the importance of this topic, the relation between the characteristics of the iron ore and its drying mechanism remains poorly understood. Furthermore, knowledge about how much water could be removed during the constant drying rate period could contribute to cost savings, because operations within this period are more energy efficient, considering the amount of energy spent per mass of water removed.

Given these issues, the aim of the present work was to characterize the granular structure and the physical and chemical properties of iron ore pellet feed and sinter feed concentrates, as well as discuss the drying kinetics of these materials. For that purpose, analyses of the chemical composition, particle size distribution, superficial area, pore structure and image analyses of the ore samples were performed. The results were related to drying kinetics data of both materials when submitted to a convective drying process and some recommendations for the design of dryers were presented.

Material and methods

Pellet feed and sinter feed

Instituto Tecnológico Vale (ITV) provided dry samples of iron ore pellet feed and sinter feed from Carajás-Brazil. These samples represent the final concentrate collected after the sieving step. The physical properties and chemical analyses (Malvern Panalytical, Zetium) of the materials are presented in Table 1.

Characterization techniques

Particle size distribution

The size distribution of the sinter feed was measured by dry screening using a sieve series from 5560 to 500 μm. The sinter feed particles smaller than 500 μm, as well as the pellet feed particles, were sized using a

Table 2. Mathematical models used to fit the experimental data of dimensionless moisture with drying time.

Model name	Model equation
Page[26]	$X^* = \exp(-kt^n)$
Newton	$X^* = \exp(-kt)$
Logarithmic[27]	$X^* = a\ \exp(-kt) + b$
Modified Page[23]	$X^* = \exp(-(kt)^n)$
Midilli[28]	$X^* = a\exp(-kt^n) + bt$
Simplified Midilli	$X^* = a\exp(-kt^n)$

Malvern Mastersizer Microplus instrument, with a minimum particle size of 0.05 μm.[22]

Surface area and pore diameter

The specific surface areas of the pellet feed and sinter feed were determined by N_2 adsorption-desorption, according to the BET method, using an ASAP 2010 analyzer (Micromeritics). All the samples were dried prior to the analysis. For the BET procedure, the sinter feed sample was sieved to two particle sizes, due to its heterogeneity: Sinter 1 (medium, d_p <1.4 mm) and Sinter 2 (fine, d_p <0.25 mm).

Pore sizes in the micrometer range were investigated by mercury porosimetry, using a PoreSizer 9320 instrument (Micromeritics). The pressure varied from 0.59 psia (0.0041 MPa) to 29,472 psia (203.20 MPa) for the mercury intrusion curve and from 27,470 psia (189.40 MPa) to 30 psia (0.21 MPa) for the extrusion, with a standard equilibration time of 10 s. The contact angle used for mercury-iron ore-air was 140°.[23,24] The specific areas of the dry materials were calculated according to the descriptions of Rootare and Prenzlow.[25]

Scanning electron microscopy

The morphologies of the materials were investigated by scanning electron microscopy (SEM), using a Philips XL-30 FEG microscope with a 15 kV electron beam at a working distance of 10.1 mm. The samples did not require coating and were randomly collected and dispersed on carbon tape before the analysis.

Experimental procedures

In order to humidify the ore, 200 g portions of the dry ore, together with the desired amounts of water, were placed in sealed polyethylene packages and kept at room temperature for 24 h.

The drying process was carried out in a forced air convection oven with air renewal system (TE-394/1, Tecnal). The air flowed parallel to the sample at a velocity of approximately 1 m/s. Assays were carried out at constant temperatures of 50, 60, 70, and 80 °C, in order to evaluate the effect of this variable on the drying kinetics of the iron ore pellet feed and sinter feed. Initial nominal moisture contents of 18 ± 0.3% and 11 ± 0.6% (wet basis) were used for the pellet feed and the sinter feed, respectively. The drying experiments were performed in triplicate, maintaining constant conditions of airflow and temperature. The process was monitored using a gravimetric method to calculate the sample moisture content according to drying time. At the end of the drying period, the samples were placed in an oven at 105 °C for 24 h, in order to determine the mass of bone dry ore.

The kinetics of the process was described using the dimensionless moisture content, calculated by:

$$X^*(t) = \frac{X_t - X_{eq}}{X_i - X_{eq}} \tag{1}$$

Considering a dry basis, X_t is the mean moisture at time t, X_i is the initial moisture, and X_{eq} is the moisture at dynamic equilibrium.

The experimental results of the dimensionless moisture with drying time were fitted to mathematical models that have been widely used in the literature to describe the kinetics of a drying process (Table 2). The coefficient of determination (R^2), reduced chi-square (χ^2), and root mean square error (RMSE) were calculated to evaluate the fitting of a model to the experimental data. High values of R^2 and lower values of χ^2 and RMSE suggest a model with a good fit to the data. These parameters were calculated by:

$$\chi^2 = \frac{\sum_{i=1}^{N}\left(X^*_{exp,i} - X^*_{pre,i}\right)^2}{N - p} \tag{2}$$

$$\mathrm{RMSE} = \left[\frac{\sum_{i=1}^{N}\left(X^*_{exp,i} - X^*_{pre,i}\right)^2}{N}\right]^{\frac{1}{2}} \tag{3}$$

where $X^*_{exp,i}$ and $X^*_{pre,i}$ are the experimental and predicted dimensionless moisture contents, respectively, N is the number of observations and p is the number of constants.

Fixed bed drying

In order to analyze the drying process under conditions closer to those of an industrial process, analysis with a fixed bed equipment were performed. Figure 1 schematically shows the experimental unit, consisting of a blower that provided air at 400 °C and 5.0 m/s to the drying chamber, which was detachable from the rig base and made of a cylindrical tube measuring 5 cm in diameter and 1 cm in height. The upstream of the drying chamber consisted of insulated carbon steel tubes.

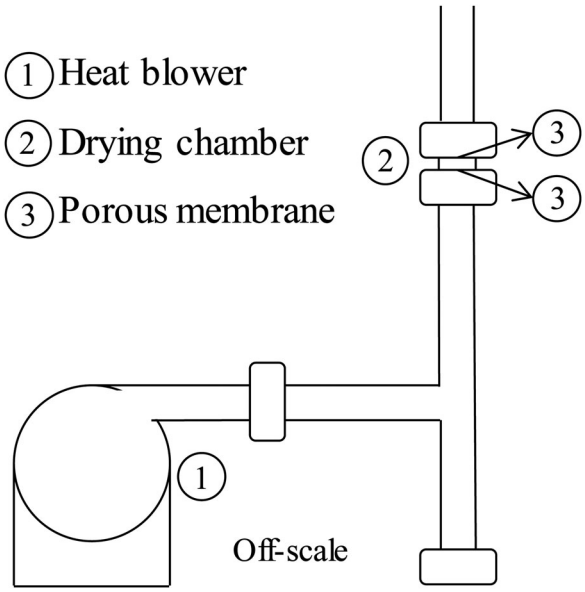

Figure 1. Experimental apparatus for drying iron ore concentrates at an air temperature of 400 °C.

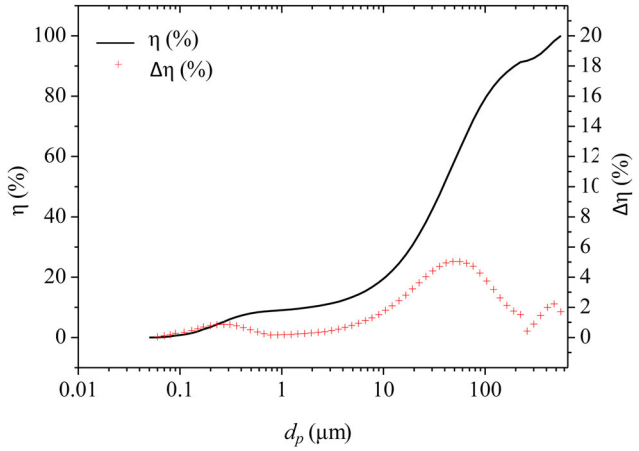

Figure 2. Cumulative particle size distribution (η) of the pellet feed.

The drying chamber was filled with the iron ore concentrates at nominal moisture of 13% and 10% for the pellet feed and for the sinter feed, respectively. These moisture contents were chosen based on operational conditions in the mining industry and to provide agglomerates suitable for the percolation of air. It must be highlighted that the moisture values used for the oven experiments (18% and 13% for pellet feed and sinter feed, respectively) are moisture levels in which two distinct phases are clearly noted, solid and liquid, e.g., a moisture grade set two percentage points higher than its saturation at 1 m effective head, for which free water is visually identified.

For each measurement, the drying chamber was detached from the rig base, then the material was quickly loaded to a glass crucible, capped to prevent moisture loss, and weighted. The moisture content was measured by the gravimetric method and the procedure was repeated for different drying times (2, 5, 10, 15, 30 and 60 s) to provide the behavior of the moisture content throughout drying. A confidence interval of 90% based on Student's t-distribution was used to define the uncertainty range of the results.

Results and discussion

Iron ore characterization

Size distribution

The particle size distributions of the pellet feed and sinter feed are shown in Figure 2 and Figure 3, respectively. Both materials presented a large quantity of ultrafine particles ($d_p < 26\,\mu m$). About 20% of the pellet feed particles were inhalable (PM_{10}), while 10% were in the $PM_{2.5}$ range. In comparison, the sinter feed presented a smaller quantity of fines, with about

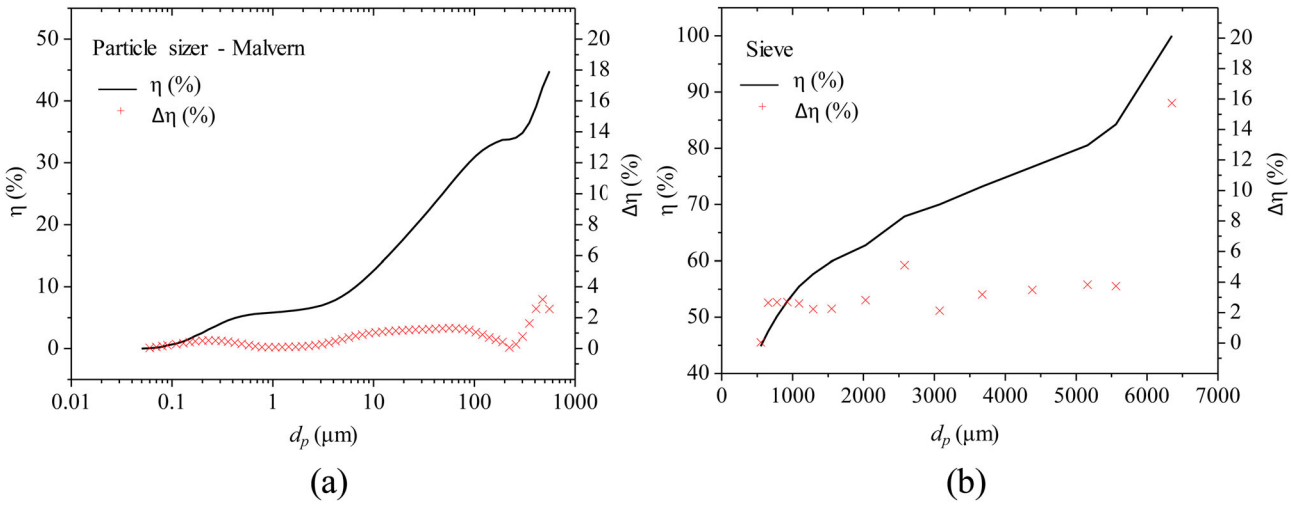

Figure 3. Cumulative particle size distribution (η) of the sinter feed: (a) Particles with d_p <500 μm analyzed using the Malvern Mastersizer Microplus instrument; (b) Particles screened using a sieve series.

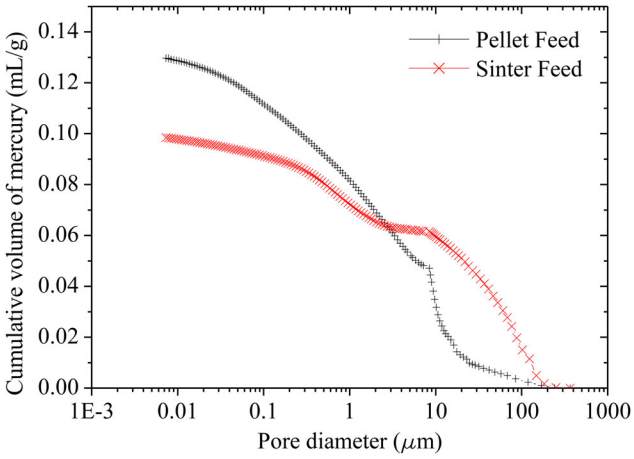

Figure 4. Results of mercury porosimetry analyses: cumulative volumes of mercury for the sinter feed and pellet feed samples.

8% of PM_{10} and 6% of $PM_{2.5}$. The results showed that the sinter feed was a mixture with about 50% of the total mass within the same size range as the pellet feed ($d_p \leq 500\,\mu m$), together with iron ore particles of larger sizes. The finer particles within the sinter feed are due to the natural generation of fines during the comminution stages. The results of this analysis suggested that during screening of the crude ore in the beneficiation process, many fines aggregated or became adhered to the larger particles, so they were not separated and remained within the sinter feed size range. The high quantities of fine particles in the compositions of the materials indicated that a large portion of the solids could be entrained into air currents if the ore with low moisture content was exposed to convection.

BET surface area

The measured surface areas of the pellet feed, medium sinter feed, and fine sinter feed were 3.88 ± 0.03, 2.42 ± 0.03, and $8.33 \pm 0.08\ m^2/g$, respectively. In BET analyses, the nitrogen adsorption technique is quantitatively limited to surface areas that are less than a few tens of square meters per gram.[29] In the current case, it could be inferred that all the materials had very low surface areas, with no substantial differences among them in terms of this property. Due to the heterogeneity in the particle diameters of the samples, together with the low surface areas, no conclusions about the shape of the pores could be obtained from the BET analyses. Furthermore, the results suggested that the observed surface areas were mainly due to particle packing (interstitial area), indicating low amounts of internal pores. According to Meyer,[5] the specific surface area depends almost exclusively on the proportions of the different sized particles, which could explain the observed results.

Mercury intrusion porosimetry

Mercury porosimetry analyses provided additional information about the pore constitution of the specific ores. The curves in Figure 4 show multimodal behavior for both materials, probably reflecting the contributions of the internal porous structure and the pores associated with compacted particles or agglomerates.[30] For the pellet feed, most of the pore volume (about 2/3) corresponded to pore diameters smaller than $8.7\,\mu m$, since the first abrupt change in the porosimetry curve occurred at this diameter. For the sinter feed, the results also indicated that larger pores were formed by the compaction of particles with sizes up to $10.0\,\mu m$, since some of this material was also in the form of a fine powder, with composition similar to that of the pellet feed. Furthermore, most of the pore volume (approximately 60%) corresponded to pore diameters greater than $10.0\,\mu m$.

The multimodal behavior observed in the porosimetry was characteristic of solid materials that agglomerated and consequently formed porous structures between the primary particles and the other ones around them.[30] In this case, the larger pores represented the interstices among the primary particles in the sample. It is noteworthy that agglomeration and compaction of the material was perceptible during handling and could be attributed to the relatively small sizes of the particles composing the powder.[30] The pellet feed was a powder with $d_p < 500\,\mu m$, which was also the case for a large volume fraction (around 50%) of the sinter feed.

The calculated specific surface areas of the pellet feed and the sinter feed were 3.1 and $1.2\,m^2/g$, respectively. The presence of compact solid materials with larger diameters and plate-like shapes in the sinter feed could help to explain the smaller area for this material. Rootare and Prenzlow[25] also observed low surface areas for iron oxide materials, with values of 14.3 and $13.3\,m^2/g$ obtained using the mercury intrusion porosimetry and BET techniques, respectively.

Porosity ratios and surface areas are key characteristics for analyzing and elucidating the mechanisms of drying systems. In the present case, the results suggested an extended period of drying at a constant rate. The BET area measurements and the mercury porosimetry data were in agreement with the iron ore measurements reported by Pena et al.[31]

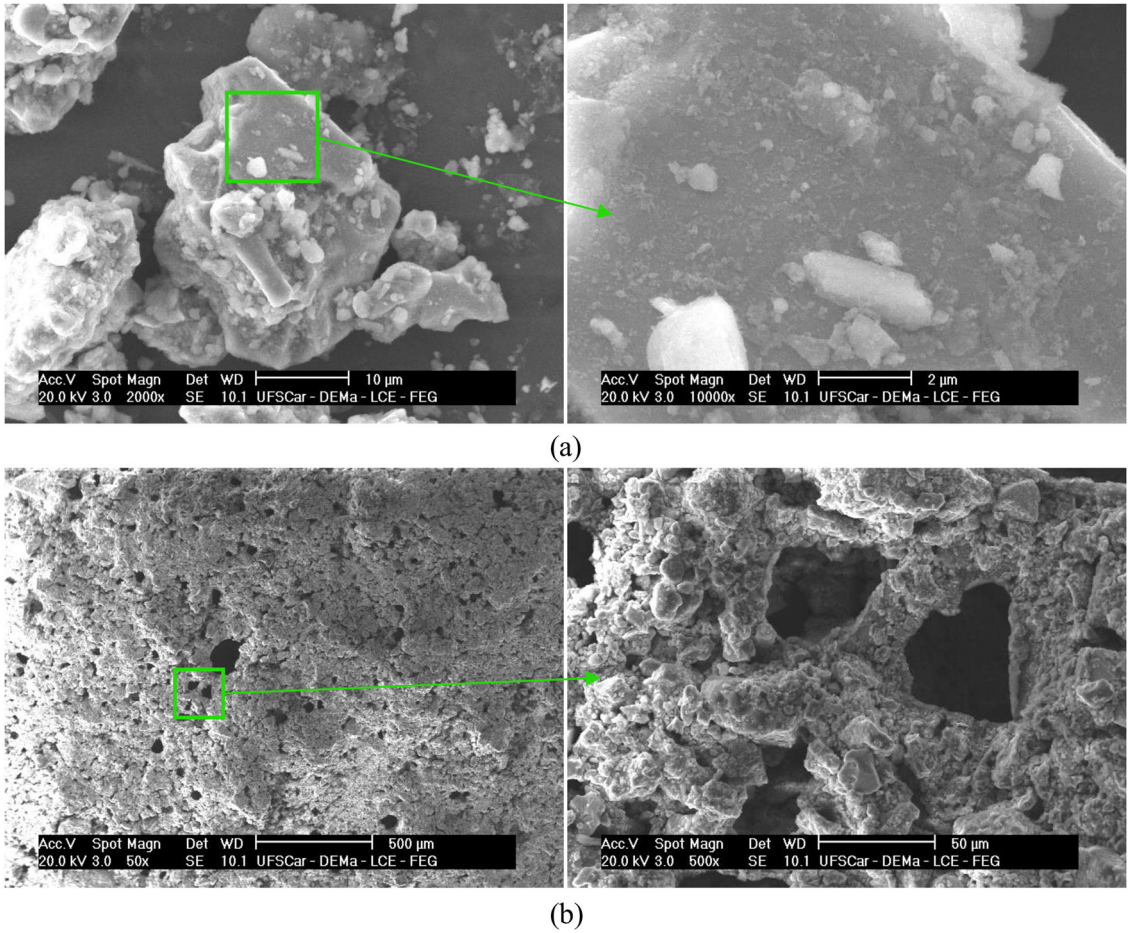

Figure 5. SEM images showing iron ore pellet feed: (a) Individual particle; (b) Agglomeration of particles formed after drying in the oven.

Particle morphology

Results from SEM indicated different arrays of Fe-bearing particles before and after drying. In the former case, the coarser particles formed discrete aggregates with finer particles (Figure 5a). The uneven and sharp cornered shape of iron ore pellet feed particles was also observed by Abazarpoor et al.[32] during SEM analysis. Hematite particles in pellet feed yielded by Vale S.A. exhibited a sphericity factor (Ψ) ranging from $\Psi = 0.2$ (plate shaped) to $\Psi = 0.5$ (roughly rounded tabular habit),[33] corroborating the SEM observations.

Figure 5(b) shows a pellet feed sample dried in the oven, which was previously humidified to a nominal moisture of 18%. The particles formed a continuous matrix permeated by voids. The SEM images show further evidence of what was discussed in the mercury porosimetry curves for pellet feed particles, i.e., Figure 5(b) on the right presents the attached fine particles and their interstices where pores with diameter less than 8.7 μm can be shown. The block of attached particles also contained some larger craters and cavities, which were possibly formed during drying, constituting the capillaries through which the water was transported from the interior to the exterior of the sample. Structural differences between the pellet feed particles were related to the size, shape, porosity, and pore structure of the particle agglomerates, which directly affect drying at moisture contents below the critical value.

Drying curves

Figure 6 shows images of the humidified materials at different moisture contents (wet basis). The pellet feed presented clear differences of consistency and cohesion, depending on the moisture values. At a nominal moisture content of 13%, the particles agglomerated and formed small blocks, while increase of the moisture to 18% led to high cohesion and formation of a uniform material, with behavior similar to that of a paste or sludge. In the case of the sinter feed, the smaller particles agglomerated at a moisture content of 11%, while at higher moisture contents, the

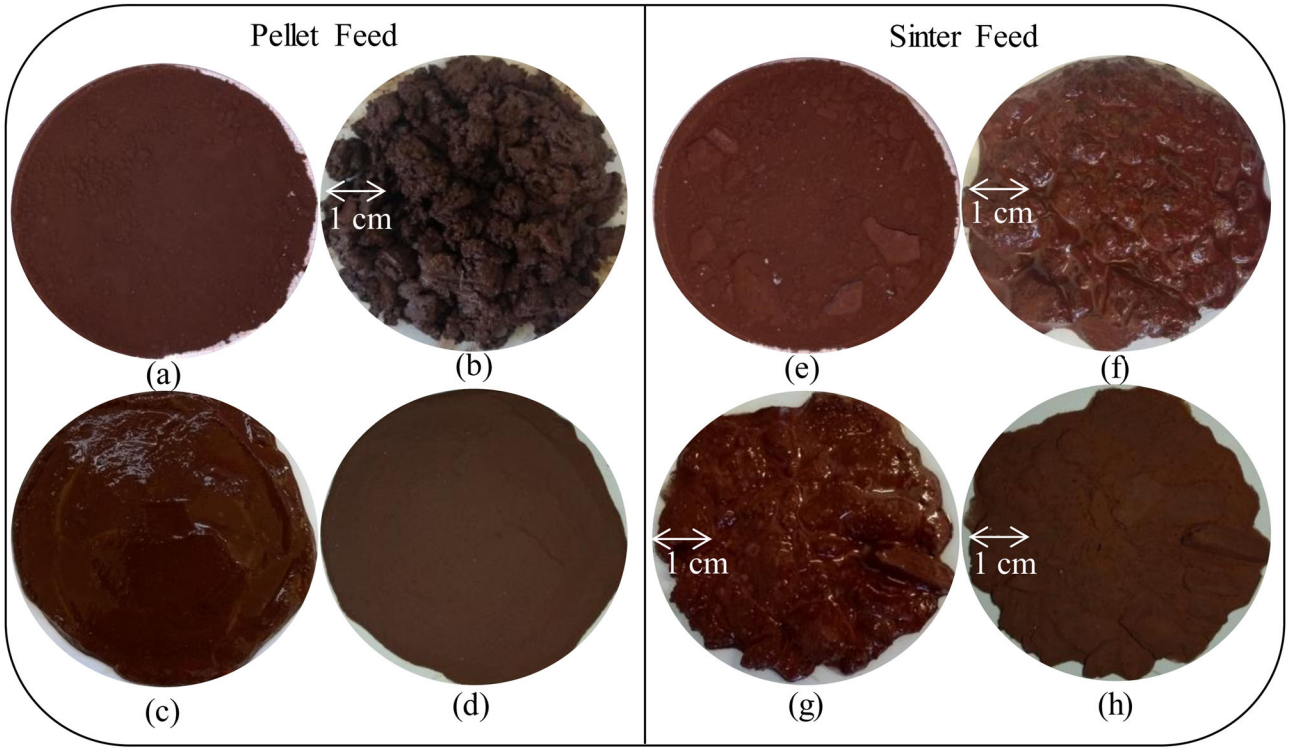

Figure 6. Images of the materials for different moisture contents and drying conditions (wet basis). Pellet feed: (a) dry (0.24%); (b) nominal moisture of 13%; (c) nominal moisture of 18%; (d) dried in the oven. Sinter feed: e) dry (0.24%); (f) nominal moisture of 13%; (g) nominal moisture of 11%; (g) dried in the oven.

material became soggy and no variation of structure could be observed visually. This behavior could be related to the saturation water content. This test applies a 1 m effective head pressure on the material. The magnitude of the saturation moisture for pellet feed and sinter feed were 16% and 11% respectively.

It should be highlighted that for both iron ores, the agglomerations remained after oven-drying for 24 h at 105 °C, after which a single block of hard dried material was formed. These findings showed that the structures of both the pellet feed and the sinter feed depended on the initial moisture content, which affected the surface area exposed to the drying air and the tendency to agglomerate.

Figure 7 shows the drying kinetics of the pellet feed and sinter feed for four different drying temperatures. The effect of temperature on drying depended on the material. For the pellet feed, a typical behavior of decreasing drying time with increasing temperature was observed, although little difference was observed between the dimensionless moisture curves for the two highest temperatures (70 and 80 °C). The drying rate curves indicated a clear increase of the drying rate with air temperature.

The sinter feed presented a typical behavior for the dimensionless moisture, with an increase in air temperature decreasing the drying time. However, the data had a higher standard deviation, compared to the dimensionless moisture curves for the pellet feed. Since the sinter feed particles presented a greater range of sizes, the surface area of each sample exposed to the drying air could present a greater variation, which in turn increased the deviation of the measurements.

As shown in Figure 7, prolonged constant drying rate periods were observed for both materials, at all temperatures, indicating that external resistance to the transport of moisture was the phenomenon that controlled the drying during most of the process. This corroborated the analyses of area and pore structure by BET and mercury porosimetry, which showed that these materials had very small pores where little moisture was retained. The periods during which the drying rate decreased were possibly due to the presence of high amounts of fine particles in the compositions of the two materials, with water being retained in the interstices of the solids and having to be transported to the surfaces, characteristic of capillary action in a non-hygroscopic porous medium. Accordingly, the materials did not show high intra-particulate porosity, indicating that the pores were formed by aggregates or clusters of compact particles (denominations according to Rouquerol et al.[34]).

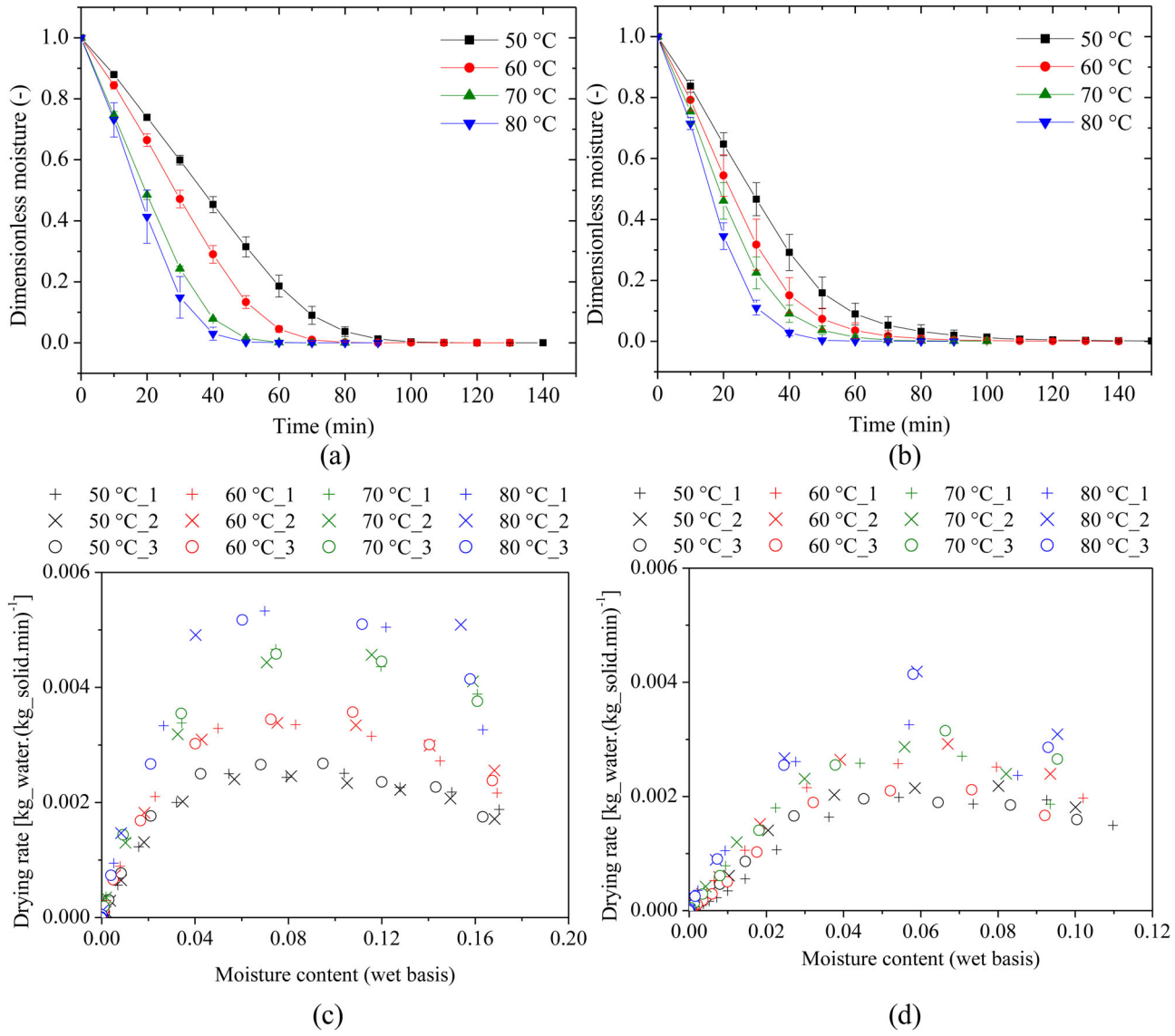

Figure 7. Drying kinetics: dimensionless moisture, as a function of drying time, for (a) the pellet feed and (b) the sinter feed; drying rate (wet basis) for (c) the pellet feed and (d) the sinter feed. Each symbol on the drying rate data corresponds to a different replica at a given temperature.

Table 3. Average values of the drying rate (wet basis) calculated at the constant rate period.

	Drying rate [kg_water.(kg_solid.min)$^{-1}$]	
Temperature (°C)	Pellet feed	Sinter feed
50	0.0023	0.0019
60	0.0031	0.0023
70	0.0043	0.0026
80	0.0050	0.0032

The behavior observed in the drying curves can be related to the pore size distribution measured in mercury porosimetry. The mercury porosimetry showed a multi-modal behavior, in which most of the pore volume for pellet feed corresponded to pore diameters less than 8.7 μm, therefore the drying behavior observed could be related to the ample size distribution of these micro-pores,[35] together with the big pores that formed craters between the "connected" particles, as was shown in Figure 5. As for the sinter feed, most of its pore volume (60%) corresponded to pore diameters greater than 10 μm (macro-pores), which favors drying. A small ratio of the pore diameter to the thickness of the viscous boundary layer[36] and evenly distributed pores are other factors that possibly contributed to maintain the product surface sufficiently wet by capillary suction, thus resulting in the ample constant rate period observed.[37]

The average drying rate values at the constant rate period are presented in Table 3. An expected increase of the drying rate with the temperature was observed for both the materials. This behavior for the iron ore

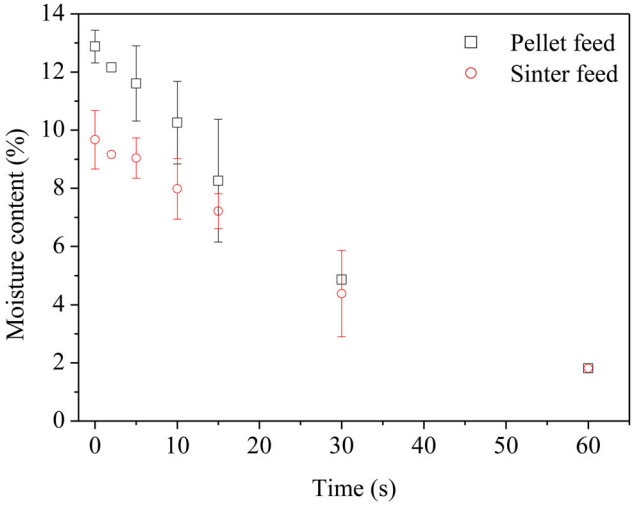

Figure 8. Drying curves for pellet feed and sinter feed in a fixed bed operating with a drying air temperature of 400 °C and an air velocity of 5 m/s. Error bars indicate a 90% confidence interval based on Student's t-distribution.

is in accordance with "Type A" materials described by Kemp and Oakley,[38] which drying rates are accelerated by higher gas temperatures.

Considering the transition between the constant rate and the decreasing rate periods in the drying rate data, the tests at all temperatures indicated critical moisture contents around 5% for the pellet feed and the sinter feed for the analyzed conditions. Given a TML value of 9.05% for iron ore materials, the results indicated that the operation of equipment designed to dry pellet feed or sinter feed could be within the constant drying rate period. This finding is particularly important for drying procedures in mining operations, considering the cost implications and the amount of energy required to reduce the moisture content of the product.

Regarding the modeling of the drying curves, Page, Modified Page, Midilli and Simplified Midilli models resulted in R^2 values greater than 0.99 for all temperatures and materials evaluated (Supplementary Table S1). Comparing the values of R^2, χ^2 and RMSE for all models, the Midilli model presented the best fit to experimental data and its parameters are shown in Supplementary Table 2. The parameter b had values very close to zero for all evaluated conditions, therefore the Simplified Midilli model was proposed, which maintained the original expression from the Midilli model, suppressing the second term on the right side. Although the Midilli model showed values of R^2, χ^2 and RMSE that indicated a better goodness of fit when compared to the Simplified Midilli model, the simplified equation presented an overall suitable fit of the experimental data using fewer constants. For this reason, the Simplified Midilli model was selected as the most adequate for describing the drying kinetics of iron ore pellet feed and sinter feed for the present study.

Outlook: Drying under industrial conditions

In the mining industry, drying temperatures up to 1000 °C are commonly used for drying ore concentrates in order to obtain high efficiency in large scale operations.[4] Contrary to what would happen to grains, seeds or fruits, for example, temperatures at this magnitude do not affect the quality of iron ore concentrates. For these reasons, an experiment with a drying temperature closer to the ones used in industrial operations (400 °C) was carried out.

Some differences between the physical phenomena of moisture removal when high or low temperatures are used in ore drying operations are worth emphasizing. Minerals are classified as nonhygroscopic capillary porous media, in which all the moisture content is unbound moisture. This kind of moisture can be removed either by evaporation or vaporization. At low temperatures, the wet solid is at a temperature below the boiling point of the liquid and moisture is transported within the product mainly by liquid diffusion. The saturation vapor pressure of the moisture on the solid is less than the atmospheric pressure and moisture is removed by vaporization. When drying at high temperatures, the vapor pressure of the moisture on the solid surface can be equal to the atmospheric pressure, therefore evaporation occurs. Furthermore, the temperature of the moisture within the solid can be raised to the boiling point and liquid vaporizes within the product, resulting in the transport of moisture by vapor diffusion.[39] In the case of high temperatures drying, the mass loss of the product can be attributed to the liberation of species other than water, e.g., carbon dioxide.

The drying kinetics of pellet feed and sinter feed at an air velocity of 5 m/s are presented in Figure 8. Although the nominal moisture of pellet feed was higher, both the materials reached approximately the same moisture level after a drying time of 30 s. Figure 8 indicates that drying rate of pellet feed was higher than that of the sinter feed in the beginning of the experiment (until around 5% of moisture content is reached). This was probably because at the nominal moisture of 13% the pellet feed formed several particle agglomerates, which increased the area of contact of the sample with the drying air.

Analyzing the drying process of Figure 8 at two stages of time, it was observed that for the first 30 s the moisture content of the pellet feed decreased about 8.0 percentage points; while the moisture of the sinter feed decreased about 5.3. On the other hand, for the last 30 s, the moisture content of the materials was lower than 5% and the contribution of internal resistances to mass transportation was more pronounced. Consequently, the removal of moisture was less than half of what was observed in the first time interval, showing a decrease of 2.5 percentage points for the pellet feed; while the sinter feed moisture decreased 2.1 percentage points. Summarizing, the equipment worked for the same time (30 s), but the removal of moisture was about 60-70% lower when the operation comprised the falling rate period.

Drying operations in mining industries have an especially high demand of energy due to the large-scale operations, as well as the high temperatures and velocities required for the drying air. Since a moderate removal of moisture from the iron ore is desired in order to prevent dusting problems,[4] these results indicated that working within the constant drying rate could result in substantially more cost-effective operations.

Observations for the design of convective dryers

Considering the characteristics of the material and the results of the drying tests discussed in this study, special attention should be given to three main factors when designing a drier for iron ore pellet feed and sinter feed: particle size distribution, solids agglomeration, and critical moisture content. Since many particles are in the PM_{10} and even $PM_{2.5}$ ranges, large amounts of solids may be entrained into the air flow and subsequently have to be collected or recovered at the air outlet. In addition, the drying may be influenced by the presence of agglomerates, due to the formation of interstitial pores. Large clusters can lead to increased critical humidity and energy consumption, unless they are disrupted by mechanical agitation or by the drying air. Therefore, it is necessary to consider the way that the material is fed, in order to maximize the surface area that comes into contact with the drying air. For example, shaft dryers are convective dryers in which the solids are "showered" through a current of the drying medium, with their flow being retarded using baffles or sieves, where necessary.[4] Furthermore, the critical moisture values observed in this study indicated that most of the drying time was during the constant drying period, offering opportunities for energy and cost savings.

Conclusions

Particle characterizations showed that the iron ore concentrates had a large amount of fine particles in the range of 8-20% with $d_p < 10\,\mu$m. BET and mercury intrusion porosimetry indicated a low surface area and volume of pores for the pellet feed and the sinter feed particles. Considering the experiments in the oven, these results supported the ample constant drying rate period observed for both materials, with critical moisture contents around 5% for the analyzed conditions. Therefore, during most of the process, the phenomenon that controlled the drying was the external resistance to the transport of moisture. The simplified Midilli model was found to be the most suitable to describe the drying kinetics of the iron ore concentrates.

The drying experiments in the fixed bed with air temperature of 400 °C showed that the removal of moisture was about 60-70% lower when the operation comprised the falling rate period. Assuming that a moderate removal of moisture is desired for the iron ore concentrates, this result indicates that drying operations within the constant rate period could imply substantial energy and cost savings.

The findings highlighted that the compositions of the ore materials included high amounts of solid fines that could form agglomerates, depending on the moisture content. Therefore, in considering the operation of a convective dryer, special attention should be given to particle feeding and collection. Furthermore, these physical characteristics may affect the removal of moisture and operational parameters such as energy consumption and the solids residence time in the dryer. Investigations in this area could help in the design of drying equipment adapted to the features of iron ore pellet feed and sinter feed, improving the energy efficiency of the process and reducing costs.

Notation

d_p	Particle diameter [m]
t	Time [s]
V_{pore}	Pore volume [m^3]
X^*	Dimensionless moisture [-]
X_{eq}	Moisture at dynamic equilibrium [$kg.kg^{-1}$]
X_t	Mean moisture at time t [s]

Greek Symbols

η	Cumulative particle size distribution [-]
$\Delta\eta$	Retained mass fraction [-]
χ^2	Reduced chi-square [-]
Ψ	Sphericity [-]

Abbreviations

RMSE	Root Mean Square Error
TML	Transportable Moisture Limit

Declaration of interest statement

No potential conflict of interest was reported by the authors.

Funding

This study was financed in part by the Coordenação de Aperfeiçoamento de Pessoal de Nível Superior – Brasil (CAPES) – Finance Code 001. This work was also supported by Conselho Nacional de Desenvolvimento Científico e Tecnológico – Brasil (CNPq) under Grant [141301/2019-8] and Grant [142102/2019-9]; and Vale S.A. - Brazil.

References

[1] United States Geological Survey (USGS). *Mineral Commodity Summaries*; USGS: Reston, VA **2019**.

[2] Organisation, I. M. (IMO). *Code of Safe Practice for Solid Bulk Cargoes*; IMO: London, **2011**.

[3] Munro, M. C.; Mohajerani, A. Determination of the Transportable Moisture Limit of Iron Ore Fines for the Prevention of Liquefaction in Bulk Carriers. *Mar. Struct.* **2015**, *40*, 193–224. DOI: 10.1016/j.marstruc.2014.11.004.

[4] Mujumdar, A. S. Chapter 42 Drying in Mineral Processing. In *Handbook of Industrial Drying*; Mujumdar, A. S., Ed.; CRC Press: Boca Raton, **2015**; pp 861–866

[5] Meyer, K. *Pelletizing of Iron Ores*; Springer-Verlag: Heidelberg; **1980**.

[6] Ljung, A. L.; Lundström, T. S.; Tano, K.; Tano, K. Simulation of Convective Drying of a Cylindrical Iron Ore Pellet. *Int. J. Numer. Methods Heat Fluid Flow* **2011**, *21*, 703–716. 10.1108/09615531111148464.

[7] Athayde, M.; Cota, M.; Covcevich, M. Iron Ore Pellet Drying Assisted by Microwave: A Kinetic Evaluation. *Miner. Process. Extr. Metall. Rev.* **2018**, *39*, 266–275. DOI: 10.1080/08827508.2017.1423295.

[8] Tan, S.; Peng, J.; Shi, H. Modeling and Simulation of Iron Ore Pellet Drying and Induration Process with Accurate Bed Void Fraction Calculation. *Dry. Technol.* **2016**, *34*, 651–664. DOI: 10.1080/07373937.2015.1070357.

[9] Ljung, A.-L.; Lundström, T. S.; Marjavaara, B. D.; Tano, K. Influence of Air Humidity on Drying of Individual Iron Ore Pellets. *Dry. Technol.* **2011**, *29*, 1101–1111. DOI: 10.1080/07373937.2011.571355.

[10] Tsukerman, T.; Duchesne, C.; Hodouin, D. On the Drying Rates of Individual Iron Oxide Pellets. *Int. J. Miner. Process* **2007**, *83*, 99–115. DOI: 10.1016/j.minpro.2007.06.004.

[11] Feng, J. X.; Zhang, Y.; Zheng, H. W.; Xie, X. Y.; Zhang, C. Drying and Preheating Processes of Iron Ore Pellets in a Traveling Grate. *Int. J. Miner. Metall. Mater.* **2010**, *17*, 535–540. DOI: 10.1007/s12613-010-0354-0.

[12] Dutra, D. C.; Emrich, M.; Magela, G.; Dias, A.; Ferrosos, C. D. T.; De; Vale, S. A.; Lima-Mg, N. Influence of Drying Temperature and Atmosphere on the Mechanical Strength of Iron-Ore Agglomerates and Sodium Silicates for Application in Sintering Processes. *Can. J. Chem. Eng*. **2016**, *94*, 75–80. DOI: 10.1002/cjce.22350.

[13] Ljung, A. L.; Staffan Lundström, T.; Daniel Marjavaara, B.; Tano, K. Convective Drying of an Individual Iron Ore Pellet - Analysis with CFD. *Int. J. Heat Mass Transf.* **2011**, *54*, 3882–3890. DOI: 10.1016/j.ijheatmasstransfer.2011.04.040.

[14] Ljung, A.; Frishfelds, V.; Lundstro, T. S.; Marjavaara, B. D. Discrete and Continuous Modeling of Heat and Mass Transport in Drying of a Bed of Iron Ore Pellets. *Dry. Technol.* **2012**, *30*, 760–773. DOI: 10.1080/07373937.2012.662567.

[15] Meer, F. P. V. D. Pellet Feed Grinding by HPGR. *Miner. Eng.* **2015**, *73*, 21–30.

[16] Wu, Z. H.; Hu, Y. J.; Lee, D. J.; Mujumdar, A. S.; Li, Z. Y. Dewatering and Drying in Mineral Processing Industry: Potential for Innovation. *Dry. Technol.* **2010**, *28*, 834–842. DOI: 10.1080/07373937.2010.490485.

[17] Krasnyi, B. L.; Tarasovskii, V. P.; Krasnyi, A. B. Development of Ceramic Material and Filtering Element Technology for Disk Vacuum Filtering Units Used in Dewatering Ferrous and Nonferrous Metal Ore Concentrates. *Refract. Ind. Ceram.* **2009**, *50*, 107–111. DOI: 10.1007/s11148-009-9156-1.

[18] Patra, A. S.; Makhija, D.; Mukherjee, A. K.; Tiwari, R.; Sahoo, C. R.; Mohanty, B. D. Improved Dewatering of Iron Ore Fines by the Use of Surfactants. *Powder Technol.* **2016**, *287*, 43–50. DOI: 10.1016/j.powtec.2015.09.030.

[19] Namkung, W.; Cho, M. Pneumatic Drying of Iron Ore Particles in a Vertical Tube. *Dry. Technol* **2004**, *22*, 877–891. DOI: 10.1081/DRT-120034268.

[20] Ghoshdastidar, P. S.; Bhargava, G.; Chhabra, R. P. Computer Simulation of Heat Transfer during Drying and Preheating of Wet Iron Ore. *Dry. Technol.* **2002**, *20*, 19–35. DOI: 10.1081/DRT-120001364.

[21] Sass, A. Simulation of Heat-Transfer Phenomena in a Rotary Kiln. *Ind. Eng. Chem. Proc. Des. Dev.* **1967**, *6*, 532–535. DOI: 10.1021/i260024a022.

[22] Litster, J. D.; Waters, A. G. Influence of the Material Properties of Iron Ore Sinter Feed on Granulation Effectiveness. *Powder Technol.* **1988**, *55*, 141–151. DOI: 10.1016/0032-5910(88)80097-4.

[23] Leitner, J. Applicationof Mercury Porosimetry in Evaluating the Quality of Iron Ore Pellets. *Powder Technol.* **1981**, *29*, 199–203. DOI: 10.1016/0032-5910(81)85017-6.

[24] Forsmo, S. P. E.; Vuori, J. P. The Determination of Porosity in Iron Ore Green Pellets by Packing in Silica Sand. *Powder Technol.* **2005**, *159*, 71–77. DOI: 10.1016/j.powtec.2005.05.032.

[25] Rootare, H. M.; Prenzlow, C. F. Surface Area from Mercury Porosimeter Measurements. *J. Phys. Chem.* **1967**, *71*, 2733–2736. DOI: 10.1021/j100867a057.

[26] Page, G. E. Factors Influencing the Maximum Rates of Air Drying Shelled Corn in Thin Layers, Purdue University, **1949**.

[27] Yaldiz, O.; Ertekin, C.; Uzun, H. I. Mathematical Modeling of Thin Layer Solar Drying of Sultana Grapes. *Energy* **2001**, *26*, 457–465. DOI: 10.1016/S0360-5442(01)00018-4.

[28] Midilli, A.; Kucuk, H.; Yapar, Z. A New Model for Single-Layer Drying. *Dry. Technol* **2002**, *20*, 1503–1513. DOI: 10.1081/DRT-120005864.

[29] Liu, P. S.; Chen, G. F. *Porous Materials, Processing and Applications*; Butterworth-Heinemann: Oxford, UK; **2014**.

[30] Giesche, H. Mercury Porosimetry: A General (Practical) Overview. *Part. Part. Syst. Charact.* **2006**, *23*, 9–11. DOI: 10.1002/ppsc.200601009.

[31] Pena, E. Q.; Antônio, C.; Gabriel, F. Caracterização Dos Parâmetros de Porosidade de Concentrados de Minério de Ferro Pelo Método de Adsorção de Nitrogênio. [Application of Nitrogen Adsorption Method for the Characterization of Porosity Parameters of Iron Ore Pellet Feed]. *Tecnol. Metal. Mater.* **2008**, *4*, 53–57. 10.4322/tmm.00404010.

[32] Abazarpoor, A.; Halali, M.; Hejazi, R.; Saghaeian, M. HPGR Effect on the Particle Size and Shape of Iron Ore Pellet Feed Using Response Surface Methodology. *Miner. Process. Extr. Metall. Rev.* **2018**, *127*, 40–48. DOI: 10.1080/03719553.2017.1284414.

[33] Souza Pinto, T. C.; Slatter, P. T.; Matai, P. H.; Leal Filho, L. S. The Influence of Hematite Particle Shape on Stratification in Pipe Flow. *Powder Technol.* **2016**, *302*, 75–80. DOI: 10.1016/j.powtec.2016.08.015.

[34] Rouquerol, J.; Avnir, D.; Fairbridge, C. W.; Everett, D. H.; Haynes, J. H.; Pernicone, N.; Ramsay, J. D. F.; Sing, K. S. W.; Unger, K. K. Recommendations for the Characterization of Porous Solids. *Pure Appl. Chem.* **1994**, *66*, 1739–1758. DOI: 10.1351/pac199466081739.

[35] Metzger, T.; Tsotsas, E. Influence of Pore Size Distribution on Drying Kinetics: A Simple Capillary Model. *Dry. Technol.* **2005**, *23*, 1797–1809. DOI: 10.1080/07373930500209830.

[36] Schlünder, E. U. Drying of Porous Material during the Constant and the Falling Rate Period: A Critical Review of Existing Hypotheses. *Dry. Technol* **2004**, *22*, 1517–1532. DOI: 10.1081/DRT-120038738.

[37] Schlünder, E. U. On the Mechanism of the Constant Drying Rate Period and Its Relevance to Diffusion Controlled Catalytic Gas Phase Reactions. *Chem. Eng. Sci* **1988**, *43*, 2685–2688. DOI: 10.1016/0009-2509(88)80012-5.

[38] Kemp, I. C.; Oakley, D. E. Modelling of Particulate Drying in Theory and Practice. *Dry. Technol* **2002**, *20*, 1699–1750. DOI: 10.1081/DRT-120015410.

[39] Mujumdar, A. S. Chapter 1 Principles, Classification, and Selection of Dryers. In *Handbook of Industrial Drying*; Mujumdar, A. S., Ed.; CRC Press: Boca Raton, **2015**; pp 3–30